Title

Drug Modulation of Water–Heme Interactions in Low-Spin P450 Complexes of CYP2C9d and CYP125A1

Journal

Biochemistry, 54(5)

ISSN

0006-2960

Authors

Conner, Kip P
Cruce, Alex A
Krzyaniak, Matthew D
et al.

Publication Date

2015-02-10

DOI

10.1021/bi501402k

Peer reviewed

HHS Public Access

Author manuscript

Biochemistry. Author manuscript; available in PMC 2015 May 19.

Published in final edited form as:

Biochemistry. 2015 February 10; 54(5): 1198–1207. doi:10.1021/bi501402k.

Drug Modulation of Water–Heme Interactions in Low-Spin P450 Complexes of CYP2C9d and CYP125A1

Kip P. Conner[†], **Alex A. Cruce**[‡], **Matthew D. Krzyaniak**[‡], **Alina M. Schimpf**[†], **Daniel J. Frank**[§], **Paul Ortiz de Montellano**[§], **William M. Atkins**[†], and **Michael K. Bowman**[*,‡]

[†]Department of Medicinal Chemistry, Box 357610, and Department of Chemistry, Box 351700, University of Washington, Seattle, Washington 98195, United States

[‡]Department of Chemistry, Box 870336, University of Alabama, Tuscaloosa, Alabama 35487, United States

[§]Department of Pharmaceutical Chemistry, University of California, San Francisco, San Francisco, California 94158, United States

Abstract

Azoles and pyridines are commonly incorporated into small molecule inhibitor scaffolds that target cytochromes P450 (CYPs) as a strategy to increase drug binding affinity, impart isoform-dependent selectivity, and improve metabolic stability. Optical absorbance spectra of the CYP–inhibitor complex are widely used to infer whether these inhibitors are ligated directly to the heme iron as catalytically inert, low-spin (type II) complexes. Here, we show that the low-spin complex between a drug-metabolizing CYP2C9 variant and 4-(3-phenyl-propyl)-1*H*-1,2,3-triazole (PPT) retains an axial water ligand despite exhibiting elements of “classic” type II optical behavior. Hydrogens of the axial water ligand are observed by pulsed electron paramagnetic resonance (EPR) spectroscopy for both inhibitor-free and inhibitor-bound species and show that inhibitor binding does not displace the axial water. A ^{15}N label incorporated into PPT is 0.444 nm from the heme iron, showing that PPT is also in the active site. The reverse type I inhibitor, LP10, of CYP125A1 from *Mycobacterium tuberculosis*, known from X-ray crystal structures to form a low-spin water-bridged complex, is found by EPR and by visible and near-infrared magnetic circular dichroism spectroscopy to retain the axial water ligand in the complex in solution.

[*]Corresponding Author: mkbowman@as.ua.edu. Telephone: (205) 348-7846.

Author Contributions

K.P.C. and A.A.C. contributed equally to this work.

Notes

The authors declare no competing financial interest.

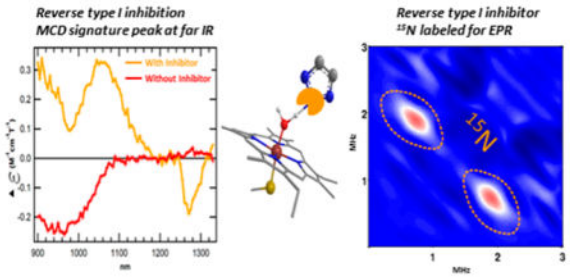

The cytochromes P450 (CYPs) comprise a large family of heme monooxygenases with diverse functions ranging from biosynthesis of sterols to detoxification of foreign chemicals and drugs. CYPs are important considerations in the design and discovery of new drugs. Human hepatic CYPs play a critical role in drug metabolism, and in addition, CYPs harbored by infectious agents are therapeutic targets. The ferric (Fe^{3+}) heme cofactor of the resting CYP is generally thought to be in equilibrium between a six-coordinate water-ligated low-spin state and a five-coordinate high-spin state. The equilibrium is isoform-dependent.[1] In the traditional paradigm, the low-spin state cannot be reduced by its physiological partner CYP reductase. Substrate binding displaces the water ligand, driving the equilibrium toward the reducible, high-spin form and allowing the catalytic cycle to start with reduction by CYP reductase. Following this paradigm, many drug design strategies incorporate imidazole, pyridine, or 1,2,4-triazole (TRZ) fragments to ligate the heme iron, trapping the low-spin CYP and preventing heme reduction. Such drugs yield optical difference spectra between drug-bound and drug-free forms, known as “type II spectra”, with a peak near 434 nm and a minimum near 410 nm, that indicate an increased fraction of low-spin heme. In most cases, crystallographic data show direct nitrogen–iron ligation with such drugs, consistent with a low-spin complex.[2,3] Drugs or inhibitors that increase the fraction of high-spin heme by displacing water without binding to the iron, but still blocking the active site, produce type I spectra that have a peak near 390 nm and a minimum near 430 nm. The terms “drug” and “inhibitor” are used interchangeably in this work and are distinguished from “ligand”, which refers to the species directly ligated to the heme iron.

These optical difference spectra are widely used to assay binding of drug candidates that target CYPs and to determine the mode of inhibition,[4] yet there are several examples that do not fit well into this spectral classification. One example is the “reverse type I” spectrum[5,6] in which the fraction of low-spin heme increases and the difference spectrum resembles type II spectra but with the minimum at 390 nm (like the peak for type I) rather than near 410 nm. The optical difference spectrum is inverted from that for type I. Weak coordination of the heme iron by the ligand heteroatom has been used to explain reverse type I spectra that are often elicited by inhibitors with heteroatoms other than sp^2-hybridized nitrogen.[6,7] However, the details of reverse type I spectra have never been fully explained. To further confuse matters, some CYP drug complexes, including some with human CYP2C9,[8] have very asymmetric difference spectra with clear troughs but minimal or absent peaks. Such spectra have never been adequately explained, although they are typically called “low-spin” complexes.

We have studied the binding of a 1,2,3-triazole (1,2,3-TRZ) derivative of estradiol, known as 17-click, with CYP3A4.[9] 17-click inhibited hydroxylation of testosterone by CYP3A4 and produced a reverse type I spectrum with a minimum at 390 nm and a maximum at 426 nm in the difference spectrum, although it was classified as type II in that paper. However, pulsed EPR measurements showed that water was the axial ligand when 17-click was bound, and the "inhibited" CYP3A4 metabolized 17-click and consumed NADPH. Thus, 17-click appears to form a hydrogen bond with the axial water ligand, while allowing enzymatic turnover in competition with other substrates. Such a binding mode, with an intact axial water ligand, is corroborated by a few CYP crystal structures.[3,10–12] It is important to determine whether similar binding modes commonly occur for other CYP isoforms and other inhibitors and to understand the functional consequences of such binding.

X-ray crystal structures can clearly reveal the presence or absence of an axial water ligand in the crystal; however, not every CYP complex can be crystallized, and the results are not always clear. The CYP121–fluconazole complex has six CYP121 molecules per asymmetric unit in the crystal.[12] Each CYP in the asymmetric unit was occupied by fluconazole to a different extent, with occupancy ranging from 0 to 100%, clouding its physiological relevance. Other methods, such as MCD and magnetic resonance, are sensitive to the axial ligand, provide moderate throughput for measurements, and can be used under conditions that are more physiologically relevant. Application of structural NMR methods to the axial ligands of oxidized CYP is limited because the paramagnetic heme broadens and shifts the NMR lines.[13] The NMR relaxation of inhibitors and substrates can reveal how molecules bind to the active site,[14–16] but it provides a structural average of all conformations and binding modes present in the sample. The pulsed and double-resonance forms of EPR directly observe ^{1}H peaks of the axial water ligand[17,18] that are shifted from peaks of most other ^{1}H's by the significant hyperfine coupling to the unpaired electron of the heme. Partial overlap with the β-^{1}H peaks of the cysteine axial ligand is revealed in one-dimensional spectra by deuteration of the solvent,[17–19] but the axial water peaks are completely resolved by pulsed EPR in 2D hyperfine sublevel correlation spectroscopy (HYSCORE) spectra.[1,9,19] The ^{1}H of axial water or other bound molecules was successfully used to study the active site structure of CYPs[1,9,19,20] and, using ^{15}N, the closely related, heme-thiolate enzyme neuronal NOS.[21,22]

In this paper, we examine complexes of a mammalian CYP2C9 variant (deletion and hepta mutant, henceforth termed CYP2C9d) and a prokaryotic CYP125A1 that behave somewhat differently from typical type II complexes. We probe the conformation and structure of the complexes using 2D HYSCORE and MCD spectroscopies. The data suggest that it may not be rare for CYP–(drug) complexes to retain water as the heme axial ligand in a hydrogen-bonded bridge to the drug, rather than displacing the water as expected of a classic type I or type II inhibitor. Our results suggest that water-bridged heme complexes can occur throughout the CYP superfamily with a range of drugs.

MATERIALS AND METHODS

Protein Preparation

CYP2C9d was constructed as previously described[23] with the substitution of a His_6 for the His_4 C-terminal tag to facilitate purification. Amino acid changes from those of the wild type were made to increase the water solubility of the enzyme. The enzyme was expressed in DL39 *Escherichia coli* and purified as described for CYP3A4.[24] CYP125A1 from *Mycobacterium tuberculosis* was prepared as previously described.[25]

Synthesis of 4-(3-Phenylpropyl)-1*H*-1,2,3-triazole (PPT)

To a 15 mL round-bottom flask containing 2 mL of a DMF/H_2O mixture (4:1) were added 144 μL of 5-phenyl-1-pentyne (0.95 mmol), 252 μL of azidotrimethylsilane (1.89 mmol), and 95 mg of sodium L-ascorbate (478 μmol). The reaction flask was sealed and placed under argon while its contents were stirred vigorously prior to the addition via syringe of 31 mg of cuprous sulfate (58 μmol) dissolved in reaction solvent. The mixture was allowed to react overnight at 70 °C. For initial workup of the reaction crude, ~1 g of florisil was added to the mixture to bind the majority of the copper ion, prior to vacuum filtration. The resin was rinsed with ~2 volumes of ethyl acetate; the organic layer was isolated; and 10 volumes of water were added to remove the DMF by liquid–liquid extraction. The organic layer was treated with saturated sodium chloride to remove excess water prior to the addition of solid $MgSO_4$. The organic solvent was evaporated to dryness and the PPT containing residue purified by silica gel (0.035–0.07 mm) chromatography with 5% CH_3OH in a CH_2Cl_2 isocratic mobile phase to afford pure PPT in 50% yield. For the synthesis of isotopically labeled [^{15}N]PPT-containing nitrogen enrichment at either N1 or N3 in a 50:50 ratio, TMS-^{15}N=N=N/TMS-N=N=^{15}N was substituted for natural abundance azidotrimethylsilane: ^{1}H NMR ($CDCl_3$) δ 2.03 (2H, m), 2.69 (2H, d, J = 7.7 Hz), 2.78 (2H, d, J = 7.8 Hz), 7.16–7.22 (3H, m), 7.25–7.32 (2H, m), 7.51 (1H); MS [M + H] = 188.2. [^{15}N]PPT: NMR ($CDCl_3$) δ 7.51 (1H, d, J_{2HN} = 6.5 Hz), 7.52 (1H, d, J_{3HN} = 4.9 Hz); ^{13}C NMR δ 24.68, 30.85, 35.39, 126.09, 128.55, 128.61, 131.65, 141.74, 147.01; MS [M + H] = 189.2.

Synthesis of ^{15}N-Labeled Trimethylsilyl-azide (TMS-^{15}N=N=N or TMS-N=N=^{15}N)

A three-neck 50 mL round-bottom flask was connected to a reflux condenser and fitted with an inline desiccant-filled drying tube attached to an oil bubbler to allow positive pressures to escape the reaction mixture. The reaction vessel was purged with argon prior to charging with 1 g of NaN_3 [^{15}N(1)] (14.8 mmol), and 10 mL of diglyme with vigorous stirring. The vessel was then sealed, set in an ice bath, and placed under a positive pressure of argon prior to addition of 1.8 mL (14.2 mmol) of trimethylsilyl chloride dropwise via syringe. The sealed reaction mixture was heated in an oil bath to 70 °C and allowed to react for 60 h. The pure product was isolated from the resultant slurry in 90% yield by vacuum distillation (8 mmHg) without heating: ^{1}H NMR ($CDCl_3$) δ 0.28 (9H, s); ^{15}N NMR (rel. liquid NH_3) δ 169.2 (s), 206.7 (s).

UV–Vis Absorbance Analysis of Inhibitor Binding

Absorbance measurements were conducted on an Olis Modernized Aminco DW-2 (Olis, Inc., Bogart, GA) dual-beam spectrophotometer equipped with a Julabo F30-C compact refrigerated circulator (Julabo USA, Inc., Allentown, PA). Each binding experiment required an initial sample volume of 500 μL using a 0.1 cm × 1 cm path length quartz cuvette, and the typical sample consisted of 1–2 μM purified CYP in 100 mM KP_i buffer and 20% glycerol. Spectra were recorded in the absolute mode (270–650 nm) between addition of 1 μL aliquots of the inhibitor stock solution not to exceed 2%/volume of organic cosolvent. Because of the excessive absorbance of LP10 during titration of CYP125A1, difference spectra were collected directly using a split cuvette format (data not shown). Affinity, K_s, and B_{max} parameters were estimated from nonlinear regression analysis in IGOR pro 6.1 (Wavemetrics, Lake Oswego, OR) using $\Delta Abs = [E{\cdot}L] = (B_{max}[L])/(K_s + [L])$.

EPR Spectroscopy

Continuous wave (CW) EPR spectra were measured on a Bruker ELEXSYS E540 X-band spectrometer with an ER 4102 ST resonator. Unless otherwise noted, CW spectra were measured at a nominal microwave frequency of 9.45 GHz with 0.42 mW of power using 100 kHz magnetic field modulation with an amplitude of 1.00 mT. Spectra were recorded at 77 K using a liquid nitrogen quartz insertion Dewar or at lower temperatures with a Bruker ER 4112 HV helium flow cryostat. EPR samples were prepared from 50 μL of a 150 μM protein solution [100 mM potassium phosphate (pH 7.4) and 20% glycerol] by the addition of 1 μL of an inhibitor-containing stock solution or the appropriate vehicle (methanol for PPT; dimethyl sulfoxide for LP10). The final inhibitor concentration was ≥350 μM for PPT or LP10 and ≥50 mM for 1,2,3-TRZ. The sample solution was placed in 3 mm outside diameter quartz EPR tubes, quickly frozen in liquid nitrogen, and stored in liquid nitrogen.

CW spectra were analyzed using EasySpin[26] to obtain g values, g strain, and the fraction of each distinct species in the sample. EPR spectra shift position if the measuring microwave frequency is changed, which can present problems in comparing pulsed and CW EPR measurements made with different spectrometers. However, for systems such as low-spin CYPs, the ratio of microwave frequency to magnetic field is a constant property of the EPR spectrum characterized by the g factor and is used to identify features in the spectrum. The spectral feature of low-spin CYP at the lowest magnetic field has the largest g factor and is called g_z, while the highest-field feature is labeled g_x; g_y is intermediate. The g factors provide a unique description of pulsed EPR measurement conditions.

Pulsed EPR measurements were taken at 15 K with a nominal microwave frequency of 9.76 GHz at different g values across the low-spin CYP spectrum with an ELEXSYS E680 EPR spectrometer (Bruker-Biospin, Billerica, MA) equipped with a Flexline ER 4118 CF cryostat and ER 4118X-MD4 ENDOR resonator. The pulsed EPR technique known as HYSCORE was used to measure ENDOR frequencies (NMR frequencies shifted by hyperfine interactions with the low-spin heme) of ^1H or ^{15}N near the heme in a 2D spectrum similar to COSY in NMR. HYSCORE uses a four-pulse microwave sequence ($\pi/2–\tau–\pi/2–t_1–\pi–t_2–\pi/2–\tau$–echo, where $\pi/2$ and π indicate pulses nominally 16 and 32 ns long that rotate the electron spin through angles of $\pi/2$ and π, respectively, while τ, t_1, and t_2 indicate delays

between pulses. The echo indicates the measured signal. This sequence was repeated at a rate of 2 kHz as t_1 and t_2 were independently incremented.[27,28] The signals from ^{1}H of the axially bound water or from ^{15}N of PPT were optimized by adjustment of τ.[9] Unless otherwise noted, a value of 240 ns was used for τ. HYSCORE cross-peaks appear in pairs at coordinates whose frequencies correlate ENDOR transitions of a single nucleus for different values of the heme unpaired electron spin.[29] Difference HYSCORE spectra were obtained by subtracting spectra after normalization to the most intense peak in the spectrum (a heme pyrrole nitrogen).[19] HYSCORE spectra are simulated with a program developed in the MATLAB environment (MathWorks, R2013b) that takes into account (1) the anisotropic g factor, (2) anisotropic hyperfine interaction, and (3) Euler rotations relating the hyperfine interaction to the g factor and the molecular frame.[17,30] Each HYSCORE spectrum measures only a limited range of orientations of the CYP relative to the magnetic field, an effect commonly known as orientation selection.[31] The distance and orientation of the water hydrogens relative to the heme were determined by global simulations of multiple HYSCORE spectra across the entire CYP EPR spectrum. The hydrogen nuclei lie in the direction of the anisotropic hyperfine interaction, A_z in megaHertz, at a distance, $R = [(14.154 g_n g_e)/A_z]^{1/3}$ in nanometers, from the heme iron.

Magnetic Circular Dichroism

MCD spectra were collected in the 6 T field of an Aviv 40DS spectropolarimeter with a high-field superconducting magneto-optical cryostat (Cryo-Industries SMC-1659 OVT) equipped with a variable-temperature sample compartment. MCD intensities are the differential absorbance of left (σ^-) and right (σ^+) circularly polarized light ($\Delta A = A_L - A_R$), following the sign convention of Piepho and Schatz,[32] in units of θ(millidegrees) = 32982 × ΔA. Data collection and sample preparation were as previously described[1] except that 1 μL (1.1%) of a DMSO stock solution of LP10 (100 mM) was added for a final inhibitor concentration of 1.1 mM (K_D = 1.7 μM[11]) to generate the reverse type I complex.

RESULTS

Identification and Characterization of the TRZ Complex in CYP2C9d

PPT produces a highly asymmetric difference spectrum in CYP2C9d with a minimum at 413 nm and no clear peak at 420–435 nm (Figure 1, top). This spectrum is distinct from the classic type II difference spectra associated with ligation of nitrogen to the heme iron, as well as reverse type I spectra, yet many groups refer to them as type II or reverse type I spectra. Similar spectra are common[8] for CYP2C9 and CYP3A4 with nitrogenous ligands and do indicate some sort of perturbation of the ligand field.

The difference spectrum for CYP2C9d with 1,2,3-TRZ (Figure 1, bottom) is a typical type II spectrum with a clear peak at 433 nm. The molar extinction coefficient of the Soret band appears to be weaker for PPT than for the 1,2,3-TRZ complex as shown by the lack of a peak in the difference spectrum for PPT (Figure 1, bottom). On the other hand, the 1,2,3-TRZ fragment and PPT both induce similar minor redshifts of the heme Soret (3 nm[9] and 4 nm, respectively) band (data not shown), and their difference spectra have similar minima.

These similarities and differences make it difficult to assess the similarity of their complexes with CYP2C9d from the difference spectra.

CW EPR spectra of drug-free CYP2C9d and complexes of CYP2C9d with 1,2,3-TRZ or PPT (Figure 2) show contributions from minor low-spin CYP species at 15 K. The spectrum of each sample was deconvoluted into individual species. The same species, as judged by their g values, can appear in more than one sample. Despite the similarities of their optical difference spectra, the two inhibitors affect the EPR g values in opposite ways (Table 1). The predominant 1,2,3-TRZ complex has a wider spectrum (and a larger spread in g values) than that of the major drug-free species, which is consistent with direct nitrogen ligation[33] to the ferric heme iron. 1,2,3-TRZ binding shifts g_z approximately +0.06 and g_x by −0.03, while PPT binding produces shifts in the opposite direction: g_z shifts −0.04, and g_x shifts +0.02, typical of ligation by an oxygen.[33]

In drug-free CYP2C9d, only two species are seen, labeled **1a** and **1b** in Table 1. Because no drug has been added, they are assigned to heme with an axial water ligand, perhaps with different arrangements of water in the active site or slightly different conformations around the active site. Addition of PPT decreases the amount of **1a** and **1b**, and a new species **2** appears. Its narrower spectrum and slightly smaller g_z are consistent with an axial oxygen ligand on the low-spin heme. However, in the sample with 1,2,3-TRZ, a species **3a** becomes the major species with the g values expected for a type II complex with 1,2,3-TRZ.

CYP125A1 Complex with Reverse Type I Inhibitor LP10

CYP125A1 from *M. tuberculosis* forms a reverse type I complex with the pyridine-based inhibitor LP10 with a minimum at 390 nm and a maximum at 422 nm in the difference spectrum.[11] Interestingly, the crystal structure of the CYP125A1–(LP10) complex [Protein Data Bank (PDB) entry 2XC3] includes a network of hydrogen-bonded water molecules between LP10 and the heme:[11] the pyridyl nitrogen of LP10 is hydrogen-bonded to a water molecule that is hydrogen-bonded to the axial water ligand of the heme. It was suggested that LP10, instead of displacing the axial water ligand, actually stabilizes the water network in the very hydrophobic active site, increasing the low-spin fraction from 20–30 to ~100%.[11]

CW EPR spectra of CYP125A1, drug-free and complexed with LP10, are very similar (Figure 3), although we found their optical spectra to be clearly different.[11] The drug-free enzyme has g_z, g_y, and g_x values of 2.401, 2.243, and 1.926, respectively, that shift very slightly to 2.395, 2.242, and 1.927, respectively, for the LP10 complex; they are quite different from the g values reported for imidazole bound in a type II complex to CYP125A1 (2.53, 2.26, and 1.89, respectively).[34] The direction of the shifts and a sharpening of the g_z peak are analogous to those observed for the CYP2C9d–(PPT) and CYP3A4–(17-click)[9] complexes and suggest a water-ligated heme similar to, but distinct from, that in the resting enzyme.

HYSCORE of ^{1}H on the Axial Water Ligand

The hydrogens of the axial water ligand were first observed in low-spin CYP in ENDOR and ESEEM spectra[17] but are difficult to resolve clearly from other hydrogens near the

heme, particularly β-hydrogens of the other axial cysteine ligand. The 2D pulsed EPR HYSCORE measurement can resolve the signals from hydrogens of the axial water ligand and can locate the hydrogens relative to the low-spin ferric heme iron.[1,9,19] The HYSCORE spectral region from hydrogens has a set of arcs from the axial water ligand (with simulated line shape in green) in drug-free CYP2C9d (Figure 4), and an additional pair of arcs from the β-hydrogens of cysteine. The water arcs disappear in D_2O, but not those from the β-hydrogens (data not shown). After binding of 1,2,3-TRZ in a classic type II complex, the water arcs disappear, showing replacement of the axial water.[1,9,19] However, the water arcs do not disappear in the CYP2C9–(PPT) and CYP125A1–(LP10) complexes (Figure 4).

HYSCORE spectra measured at different *g* values differ because the magnetic field changes at each *g* value and because the spectra arise from hemes with different orientations relative to the magnetic field, a phenomenon known as orientation selection. The entire set of spectra was simulated for each sample, varying hyperfine couplings and orientations of water hydrogens relative to the heme. Simulated and experimental spectra are compared at three different *g* values for each sample in Figure 4. The axial water ligand remains in the reverse type I complexes, and the location of the water hydrogens is only slightly perturbed (Table 2). The polar angles, defined in Figure 5, for the hydrogens of the water show only a modest rotation of the water around the Fe–O coordination bond.

The small changes in the position of the axial water could arise from binding of the inhibitor away from the active site, e.g., at an allosteric site. To verify the location of the inhibitor, PPT was isotopically labeled with ^{15}N in a 50:50 mixture at the 1 and 3 positions of triazole. Two new peaks with moderate ^{15}N hyperfine couplings appear in the HYSCORE spectrum and are quite prominent in the difference HYSCORE spectra (Figure 6), with loss of intensity from some ^{14}N peaks because of replacement of ^{14}N by the ^{15}N label. Simulated ^{15}N spectra (contours) with the nitrogen label at 0.444 nm from the heme iron show that both the nitrogen from PPT and the axial water hydrogens are present in the CYP2C9d–(PPT) complex. For comparison, the distance between Fe and the 1,2,4-triazole nitrogen that is hydrogen-bonded to the axial water ligand in the CYP121–(fluconazole) crystal structure (PDB entry 2IJ7) is 0.435 nm.[12] While this distance suggests a hydrogen bond with N1 or N3 of PPT, a bond with N2 might be possible for a different inhibitor conformation.

MCD of the CYP125A1–(LP10) Complex

In a comparison of drug-free CYP and its water-bridged complexes, the CW EPR and HYSCORE spectra indicate very similar coordination of the heme iron while optical difference spectra have changes comparable to those caused by replacement of water in type II complexes. To understand these conflicting results, MCD spectroscopy was applied to the CYP125A1–(LP10) complex that can be easily saturated to give a single, low-spin species as shown by EPR in both drug-free and LP10-saturated states (Figure 3). The CYP125A1–(LP10) complex has two water molecules forming a hydrogen-bonded network between the heme and the pyridine group of LP10 (PDB entry 2XC3)[11] in contrast to the single bridging water reported in the CYP121A1–(fluconazole) complex[34] and found here in the CYP2C9–

(PPT) complex or, alternatively, with no obvious connection in the CYP101A1–(2-PI)[3] complex (PDB entry 1PHE).

The visible (500–750 nm) and near-infrared (900–1350 nm) MCD spectra for both drug-free[1] and LP10-saturated CYP125A1 at 298 and 4.2 K (Figure 7 and Table 3) are remarkably different. The visible α and β heme bands (500–750 nm) at 298 K show that saturation of the predominantly high-spin isoform with LP10 converts it to a predominantly low-spin state. The main low-spin features at 518, 558, and 574 nm have wavelength and molar absorptivity values (Table 3) extremely close to those of drug-free bacterial CYP101A1 (518, 558, and 575 nm, respectively)[33] in its H_2O-ligated, low-spin resting state.[17,18,35,36] This result corroborates that the axial water ligation of the CYP125A1–(LP10) complex persists outside the crystal, because nitrogen donors that ligate the CYP iron directly cause significant MCD spectral shifts. For example, pyridine shifts these features to 525, 560, and 580 nm, respectively, concomitant with large decreases in MCD intensity.

The ligand-to-metal charge transfer (LMCT) bands in the near-infrared MCD spectrum can help assign axial ligands, because their energy uniquely reports axial and rhombic distortions of the ligand field by the distal sixth ligand.[37,38] Nitrogenous drugs that ligate heme iron shift this band to much lower energies. In type II complexes of CYP3A4 with imidazole and 1,2,3-triazole-based inhibitors, we observe (data not shown) a 50–100 nm redshift of the LMCT band from its drug-free value of 1050 nm. The low-spin LMCT band of drug-free and LP10-saturated CYP125A1 cannot be compared at room temperature because the drug-free form is predominantly high-spin and its LMCT band is not reliably seen. However, the LMCT band of the CYP125A1–(LP10) complex is close to that of drug-free CYP3A4, suggesting they have similar heme ligands and that the CYP125A1–(LP10) complex in a room-temperature solution maintains the water-bridged structure seen in the crystal.

The MCD measurements at 4.2 K are more revealing because the low-spin signal at cryogenic temperatures is amplified relative to that in the high-spin enzyme. This allows comparison of MCD features of the drug-free and LP10-saturated enzyme in both the visible and near-infrared regions. The visible MCD spectra (Figure 7, top right) are similar, but the small differences for all the major peaks show that LP10 is bound. Formation of the complex with LP10 is perhaps most evident by comparison of the negative band fine structure between 640 and 720 nm (Figure 7, left inset) known to contain features from the high-spin enzyme diagnostic of the high-spin ligand field. Type II compounds typically shift the near-infrared peak at 1040 nm by 50–80 nm, while LP10 binding produces virtually no shift, consistent with the ~5 nm blue shift predicted[38] from the measured EPR g values. In addition, the band intensity is dramatically diminished by binding of LP10, which also occurred in the room-temperature MCD spectrum of the CYP121–(fluconazole) complex.[12] Is is worth noting that the empirical correlation between the near-infrared LMCT band intensity and heme ligand field rhombicity is supported by a theoretical treatment.[39]

DISCUSSION

A remarkably consistent picture emerges for the CYP2C9d–(PPT) and CYP125A1–(LP10) complexes and the previously studied CYP3A4–(17-click) complex[9] from MCD, EPR, HYSCORE, and crystallography studies. When the inhibitor binds, the axial water ligand of the inhibitor-free enzyme, in each case, remains in place and participates in a hydrogen-bonded water bridge between the heme iron and the inhibitor. The MCD and CW EPR spectra show that binding produces little change in the ligand field of the heme, far less than would replacement of the water by a nitrogen from the ligand. The HYSCORE spectra clearly show that the water hydrogens are intact and are not displaced from the active site. At the same time, the perturbations of the EPR spectra indicate that the inhibitor does have some effect on the active site. The crystal structure of the CYP125A1–(LP10) complex[11] and the detection of ^{15}N HYSCORE peaks in the CYP2C9d–([^{15}N]PPT) spectra conclusively place the inhibitor in the active site rather than at some hypothetical allosteric site in the protein.

Unfortunately, things are not so clear-cut in the optical difference spectra used for high-throughput screening in drug development.[4] The difference spectra of these water-bridged complexes resemble the classic type II difference spectra closely enough that they are often classified as type II. Such was the case in our initial study of the CYP3A4–(17-click) complex that we originally called a type II complex[9] but is more accurately classified as a reverse type I complex. Incorrect classification of a complex as type II can cause misconceptions about the mode of interaction because of the widespread assumption that all type II complexes involve displacement of the axial water ligand by a stronger ligand, with nitrogen directly coordinated to the heme. This new binding mode adds a layer of structural complexity to the discussion of drug-induced heme spin-state perturbations, and of the catalytic competency of low-spin CYP complexes. There are limitations to a rigid CYP–drug classification paradigm in which all nitrogen heterocycle-containing drugs are assumed to behave identically with respect to the heme.

These limitations are readily seen in the deconvolution of the CW EPR spectra of CYP2C9d (Table 1). The CYP2C9d–(PPT) sample contains **1a** and **1b** species seen in the drug-free sample with a new species **2**. The narrow spectrum and slightly smaller g_z of species **2** are consistent with an axial oxygen ligand on the low-spin heme. There is, in addition, ~15% of a species **3a** with a substantially wider EPR spectrum and larger g_z, which appears to be consistent with a small amount of low-spin heme with an axial nitrogen ligand (as would be expected of a true type II complex). Thus, the CYP2C9d–(PPT) sample seems to contain the major water-bridged complex along with minor amounts of water- and nitrogen-ligated structures. Furthermore, in the CYP2C9d–(1,2,3-TRZ) sample, species **3a** becomes the major species with small amounts of **3b**, which also has the g values expected of a type II complex, along with some residual **1b** where 1,2,3-TRZ does not seem to be bound at all. It appears that CYP2C9d is able to accommodate PPT and 1,2,3-TRZ in several different conformations, in equilibrium with each other.

The optical binding isotherms that clearly show binding of PPT to CYP2C9d are readily interpreted as indicating type II binding, which could have important consequences. Several

triazole derivatives bind and inhibit CYP2C9 in human studies as well as *in vitro*. Our CW EPR studies show that interactions of the inhibitor with CYP2C9 may not be simple, making it important to understand those interactions relative to CYP2C9 activity, especially for triazole-based drugs.[40,41]

The results for CYP2C9d emphasize the problem with optical difference spectra. The complexes of CYP2C9d with 1,2,3-TRZ and PPT have very similar optical difference spectra, highly asymmetric with a distinct minimum at 410–413 nm but with little or no maximum near 433 nm, which are distinct from either type II or reverse type I spectra, yet EPR and HYSCORE measurements indicate that 1,2,3-TRZ has a nitrogen directly bound to the heme as expected for a type II complex while PPT exhibits water-bridged heme binding. A major reason for such varied results is that at least three effects interact to produce the optical difference spectrum: (1) a shift in the equilibrium between high- and low-spin heme, resulting in changes in the intensity of each of their Soret bands, (2) a redshift in the Soret band of the low-spin heme caused by changes in the heme ligand field, and (3) changes in the extinction coefficient of the low-spin heme Soret band. It is possible to find indications of all three effects operating in the systems studied here.

The results for CYP2C9d and CYP125A1 presented here extend previous observations of the CYP3A4–(17-click) complex. It now becomes clear that water-bridged structures are not limited to a unique drug or a single CYP and in fact may be common. We find obvious similarities between our data and the EPR signatures reported by Dawson[33] for a series of sterically hindered nitrogen heterocycles [indole, benzimidazole, and 2-phenylimidazole (2-PI)] in complex with P450cam, which were simply categorized as “abnormal” N donors.[33] Poulos et al.[3] later reported that the crystal structure of the P450cam–(2-PI) complex (PDB entry 1PHE) does contain an axial water ligand but without any obvious hydrogen bonding route to the 2-PI nitrogen. An additional crystallographic example is CYP121 in complex with a *cyclo*-dityrosyl substrate (PDB entry 3G5H[10]) that has a complex heme–H_2O–inhibitor structure involving as many as three structural waters in H-bonding contact with the inhibitor, including the axial H_2O ligand of the heme.

It could be argued that the CYP125A1–(LP10) structure might be driven by a steric clash within the tight active site that controls access to the heme iron,[11] but the structural simplicity of PPT makes a similar explanation seem unlikely for the CYP2C9d–(PPT) complex. The CW EPR spectra show that a variety of binding motifs coexist, including a water-bridged structure with a nitrogen-containing drug. Although CW EPR and MCD spectra can detect the presence of an axial water ligand on the basis of the size and shape of spectral shifts, they do not seem to be able to identify the exact binding motif.

The water-bridged CYP3A4–(17-click) complex is catalytically competent to modify the 17-click inhibitor,[9] although its normal activity was inhibited, while the low-spin CYP2C9d–(PPT) and CYP125A1–(LP10) complexes studied here are metabolically stable (data not shown). The CYP3A4–(17-click) complex produced a small “library” of modified inhibitors with potential to cause a wide range of side effects. Finding that the CYP2C9d–(PPT) complex has a similar water-bridged structure carries important implications for CYP2C9 and other CYPs involved in drug metabolism. Water-bridged drug–CYP complexes that

retain catalytic activity, as does CYP3A4 with 17-click, could lead to unanticipated metabolism. The H-bond donation from the axial H_2O in CYP to an azole drug may impart more hydroxide-like (high-spin) character to the heme iron that encourages more facile reduction of the cofactor. Such a mechanism has been suggested by Jones et al.[42] to explain facile turnover of several type II binding pyridines, but without consideration of the water-bridged structures revealed by this study.

Acknowledgments

Funding

This work was supported by National Institutes of Health (NIH) Grants 1R01 GM110790 (W.M.A.) and T32 GM007750-36 (K.P.C.), National Science Foundation Grant DGE1256082 (A.M.S.), and NIH Grants AI074824 and GM25515 (P.O.d.M.).

ABBREVIATIONS

2D	two-dimensional
17-click	17*α*-(2*H*-2,3,4-triazolyl)-estradiol
COSY	correlation spectroscopy
CW	continuous wave
CYP	cytochrome P450
DMF	dimethylformamide
DMSO	dimethyl sulfoxide
ENDOR	electron nuclear double resonance
EPR	electron paramagnetic resonance
HYSCORE	hyperfine sublevel correlation spectroscopy
LMCT	ligand-to-metal charge transfer
LP10	*α*-[(4-methylcyclohexyl)carbonyl amino]-*N*-4-pyridinyl-1*H*-indole-3-propanamide
MCD	magnetic circular dichroism
MS	mass spectrometry
NADPH	reduced nicotinamide adenine dinucleotide phosphate
NMR	nuclear magnetic resonance
NOS	nitric oxide synthase
PPT	4-(3-phenylpropyl)-1*H*-1,2,3-triazole
TRZ	1,2,3-triazole or 1,2,4-triazole

References

1. Conner KP, Schimpf AM, Cruce AA, McLean KJ, Munro AW, Frank DJ, Krzyaniak MD, Ortiz de Montellano P, Bowman MK, Atkins WM. Strength of Axial Water Ligation in Substrate-Free Cytochrome P450s Is Isoform Dependent. Biochemistry. 2014; 53:1428–1434. [PubMed: 24576089]
2. Ekroos M, Sjögren T. Structural Basis for Ligand Promiscuity in Cytochrome P450 3A4. Proc Natl Acad Sci USA. 2006; 103:13682–13687. [PubMed: 16954191]
3. Poulos TL, Howard AJ. Crystal Structures of Metyrapone- and Phenylimidazole-Inhibited Complexes of Cytochrome P-450cam. Biochemistry. 1987; 26:8165–8174. [PubMed: 3442650]
4. Podust LM, von Kries JP, Eddine AN, Kim Y, Yermalitskaya LV, Kuehne R, Ouellet H, Warrier T, Altekoster M, Lee JS, Rademann J, Oschkinat H, Kaufmann SHE, Waterman MR. Small-Molecule Scaffolds for CYP51 Inhibitors Identified by High-Throughput Screening and Defined by X-ray Crystallography. Antimicrob Agents Chemother. 2007; 51:3915–3923. [PubMed: 17846131]
5. Schenkman JB, Cinti DL, Orrenius S, Moldeus P, Kraschnitz R. Nature of Reverse Type I (Modified Type II) Spectral Change in Liver Microsomes. Biochemistry. 1972; 11:4243–4251. [PubMed: 5079897]
6. Kumaki K, Sato M, Kon H, Nebert DW. Correlation of Type-I, Type-II, and Reverse Type-I Difference Spectra with Absolute Changes in Spin State of Hepatic Microsomal Cytochrome-P-450 Iron from 5 Mammalian-Species. J Biol Chem. 1978; 253:1048–1058. [PubMed: 203579]
7. Shimada T, Tanaka K, Takenaka S, Foroozesh MK, Murayama N, Yamazaki H, Guengerich FP, Komori M. Reverse Type I Binding Spectra of Human Cytochrome P450 1B1 Induced by Flavonoid, Stilbene, Pyrene, Naphthalene, Phenanthrene, and Biphenyl Derivatives That Inhibit Catalytic Activity: A Structure-Function Relationship Study. Chem Res Toxicol. 2009; 22:1325–1333. [PubMed: 19563207]
8. Locuson CW, Hutzler JM, Tracy TS. Visible Spectra of Type II Cytochrome P450-Drug Complexes: Evidence that “Incomplete” Heme Coordination is Common. Drug Metab Dispos. 2007; 35:614–622. [PubMed: 17251307]
9. Conner KP, Vennam P, Woods CM, Krzyaniak MD, Bowman MK, Atkins WM. 1,2,3-Triazole-Heme Interactions in Cytochrome P450: Functionally Competent Triazole-Water-Heme Complexes. Biochemistry. 2012; 51:6441–6457. [PubMed: 22809252]
10. Belin P, Le Du MH, Fielding A, Lequin O, Jacquet M, Charbonnier JB, Lecoq A, Thai R, Courcon M, Masson C, Dugave C, Genet R, Pernodet JL, Gondry M. Identification and Structural Basis of the Reaction Catalyzed by CYP121, an Essential Cytochrome P450 in *Mycobacterium tuberculosis*. Proc Natl Acad Sci USA. 2009; 106:7426–7431. [PubMed: 19416919]
11. Ouellet H, Kells PM, Ortiz de Montellano PR, Podust LM. Reverse type I inhibitor of *Mycobacterium tuberculosis* CYP125A1. Bioorg Med Chem Lett. 2011; 21:332–337. [PubMed: 21109436]
12. Seward HE, Roujeinikova A, McLean KJ, Munro AW, Leys D. Crystal Structure of the *Mycobacterium tuberculosis* P450CYP121-Fluconazole Complex Reveals New Azole Drug-P450 Binding Mode. J Biol Chem. 2006; 281:39437–39443. [PubMed: 17028183]
13. Banci L, Bertini I, Marconi S, Pierattelli R, Sligar SG. Cytochrome P450 and Aromatic Bases: A ^{1}H NMR Study. J Am Chem Soc. 1994; 116:4866–4873.
14. Roberts AG, Yang J, Halpert JR, Nelson SD, Thummel KT, Atkins WM. The Structural Basis for Homotropic and Heterotropic Cooperativity of Midazolam Metabolism by Human Cytochrome P450 3A4. Biochemistry. 2011; 50:10804–10818. [PubMed: 21992114]
15. Cameron MD, Wen B, Roberts AG, Atkins WM, Campbell AP, Nelson SD. Cooperative Binding of Acetaminophen and Caffeine within the P450 3A4 Active Site. Chem Res Toxicol. 2007; 20:1434–1441. [PubMed: 17894464]
16. Cameron MD, Wen B, Allen KE, Roberts AG, Schuman JT, Campbell AP, Kunze KL, Nelson SD. Cooperative Binding of Midazolam with Testosterone and α-Naphthoflavone within the CYP3A4 Active Site: A NMR T_1 Paramagnetic Relaxation Study. Biochemistry. 2005; 44:14143–14151. [PubMed: 16245930]

17. Goldfarb D, Bernardo M, Thomann H, Kroneck PMH, Ullrich V. Study of Water Binding to Low-Spin Fe(III) in Cytochrome P450 by Pulsed ENDOR and Four-Pulse ESEEM Spectroscopies. J Am Chem Soc. 1996; 118:2686–2693.
18. Thomann H, Bernardo M, Goldfarb D, Kroneck PMH, Ullrich V. Evidence for Water Binding to the Fe Center in Cytochrome P450cam Obtained by ^{17}O Electron Spin Echo Envelope Modulation Spectroscopy. J Am Chem Soc. 1995; 117:8243–8251.
19. Roberts AG, Cheesman MJ, Primak A, Bowman MK, Atkins WM, Rettie AE. Intramolecular Heme Ligation of the Cytochrome P450 2C9 R108H Mutant Demonstrates Pronounced Conformational Flexibility of the B-C Loop Region: Implications for Substrate Binding. Biochemistry. 2010; 49:8700–8708. [PubMed: 20815369]
20. Davydov R, Gilep AA, Strushkevich NV, Usanov SA, Hoffman BM. Compound I Is the Reactive Intermediate in the First Monooxygenation Step during Conversion of Cholesterol to Pregnenolone by Cytochrome P450scc: EPR/ENDOR/Cryoreduction/Annealing Studies. J Am Chem Soc. 2012; 134:17149–17156. [PubMed: 23039857]
21. Tierney DL, Huang H, Martasek P, Masters BS, Silverman RB, Hoffman BM. ENDOR Spectroscopic Evidence for the Position and Structure of NG-hydroxy-L-arginine Bound to Holo-Neuronal Nitric Oxide Synthase. Biochemistry. 1999; 38:3704–3710. [PubMed: 10090758]
22. Astashkin AV, Elmore BO, Chen L, Fan WH, Guillemette JG, Feng CJ. Pulsed ENDOR Determination of the Arginine Location in the Ferrous-NO Form of Neuronal NOS. J Phys Chem A. 2012; 116:6731–6739. [PubMed: 22667467]
23. Williams PA, Cosme J, Ward A, Angova HC, Vinkovic DM, Jhoti H. Crystal Structure of Human Cytochrome P4502C9 with Bound Warfarin. Nature. 2003; 424:464–468. [PubMed: 12861225]
24. Woods CM, Fernandez C, Kunze KL, Atkins WM. Allosteric Activation of Cytochrome P450 3A4 by α-Naphthoflavone: Branch Point Regulation Revealed by Isotope Dilution Analysis. Biochemistry. 2011; 50:10041–10051. [PubMed: 22004098]
25. Ouellet H, Lang J, Couture M, Ortiz de Montellano PR. Reaction of *Mycobacterium tuberculosis* Cytochrome P450 Enzymes with Nitric Oxide. Biochemistry. 2009; 48:863–872. [PubMed: 19146393]
26. Stoll S, Schweiger A. EasySpin, a Comprehensive Software Package for Spectral Simulation and Analysis in EPR. J Magn Reson. 2006; 178:42–55. [PubMed: 16188474]
27. Maryasov AG, Bowman MK. Two-Dimensional Hyperfine Sublevel Correlation Spectroscopy: Powder Features for S = 1/2, I = 1. J Magn Reson. 2006; 179:120–135. [PubMed: 16337820]
28. Bowman, MK. Pulsed Electron Paramagnetic Resonance. In: Brustolon, M.; Giamello, E., editors. Electron Paramagnetic Resonance: A Practitioner's Toolkit. John Wiley & Sons; Hoboken, NJ: 2009. p. 159-194.
29. Dikanov SA, Bowman MK. Cross-Peak Lineshape of Two-Dimensional ESEEM Spectra in Disordered S = 1/2, I = 1/2 Spin System. J Magn Reson, Ser A. 1995; 116:125–128.
30. Maryasov AG, Bowman MK. Spin Dynamics of Paramagnetic Centers with Anisotropic g Tensor and Spin of 1/2. J Magn Reson. 2012; 221:69–75. [PubMed: 22743542]
31. Dikanov SA, Xun LY, Karpiel AB, Tyryshkin AM, Bowman MK. Orientationally-Selected Two-Dimensional ESEEM Spectroscopy of the Rieske-Type Iron-Sulfur Cluster in 2,4,5-Trichlorophenoxyacetate Monooxygenase from *Burkholderia cepacia* AC1100. J Am Chem Soc. 1996; 118:8408–8416.
32. Piepho, SB.; Schatz, PN. Group Theory in Spectroscopy with Applications to Magnetic Circular Dichroism. John Wiley and Sons; New York: 1983.
33. Dawson JH, Andersson LA, Sono M. Spectroscopic Investigations of Ferric Cytochrome P-450-Cam Ligand Complexes: Identification of the Ligand Trans to Cysteinate in the Native Enzyme. J Biol Chem. 1982; 257:3606–3617. [PubMed: 6277939]
34. McLean KJ, Lafite P, Levy C, Cheesman MR, Mast N, Pikuleva IA, Leys D, Munro AW. The Structure of *Mycobacterium tuberculosis* CYP125: Molecular Basis for Cholesterol Binding in a P450 Needed for Host Infection. J Biol Chem. 2009; 284:35524–35533. [PubMed: 19846552]
35. Poulos TL, Finzel BC, Howard AJ. High-Resolution Crystal-Structure of Cytochrome-P450cam. J Mol Biol. 1987; 195:687–700. [PubMed: 3656428]

36. Sligar SG. Coupling of Spin, Substrate, and Redox Equilibria in Cytochrome P450. Biochemistry. 1976; 15:5399–5406. [PubMed: 187215]

37. Gadsby PMA, Thomson AJ. Assignment of the Axial Ligands of Ferric Ion in Low-Spin Hemoproteins by near-Infrared Magnetic Circular-Dichroism and Electron-Paramagnetic Resonance Spectroscopy. J Am Chem Soc. 1990; 112:5003–5011.

38. Taylor CPS. EPR of Low-Spin Heme Complexes: Relation of t_{2g} Hole Model to Directional Properties of g-Tensor, and a New Method for Calculating Ligand-Field Parameters. Biochim Biophys Acta. 1977; 491:137–149. [PubMed: 191085]

39. Thomson AJ, Gadsby PMA. A Theoretical-Model of the Intensity of the near-Infrared Porphyrin-to-Iron Charge-Transfer Transitions in Low-Spin Iron(III) Hemoproteins: A Correlation between the Intensity of the Magnetic Circular-Dichroism Bands and the Rhombic Distortion Parameter of Iron. J Chem Soc, Dalton Trans. 1990:1921–1928.

40. Pearson MM, Rogers PD, Cleary JD, Chapman SW. Voriconazole: A New Triazole Antifungal Agent. Ann Pharmacother. 2003; 37:420–432. [PubMed: 12639175]

41. Hyland R, Jones BC, Smith DA. Identification of the Cytochrome P450 Enzymes Involved in the N-Oxidation of Voriconazole. Drug Metab Dispos. 2003; 31:540–547. [PubMed: 12695341]

42. Pearson J, Dahal UP, Rock D, Peng CC, Schenk JO, Joswig-Jones C, Jones JP. The Kinetic Mechanism for Cytochrome P450 Metabolism of Type II Binding Compounds: Evidence Supporting Direct Reduction. Arch Biochem Biophys. 2011; 511:69–79. [PubMed: 21530484]

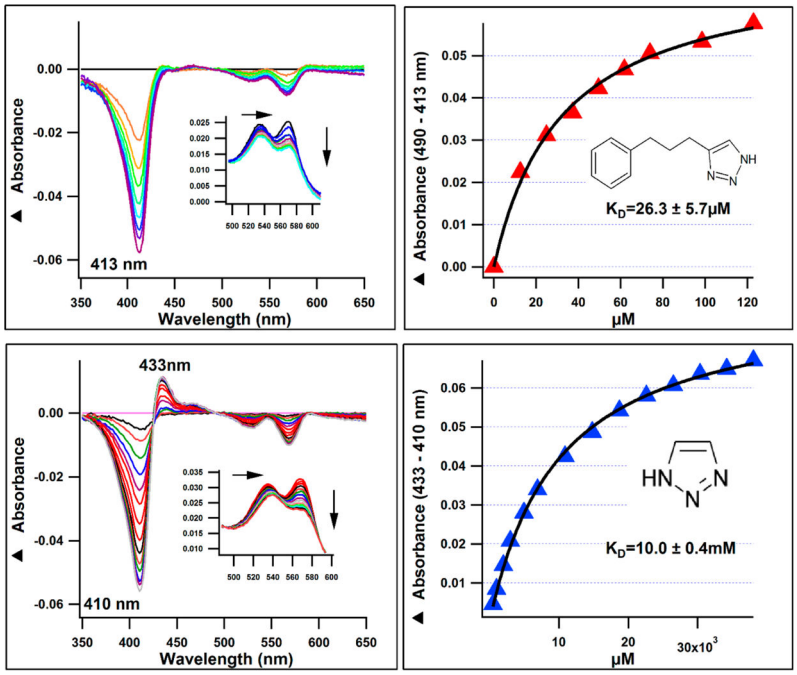

Figure 1.

Absorbance difference spectra (left) and binding isotherm (right) for CYP2C9d with PPT (top) and 1,2,3-TRZ (bottom). Note the lack (top left) of the positive peak observed previously in the Soret region (350–470 nm) with other nitrogenous ligands for CYP2C9.[8] The *α*/*β* bands in the absolute absorbance spectra in the inset are similar to those found in classic type II spectra.

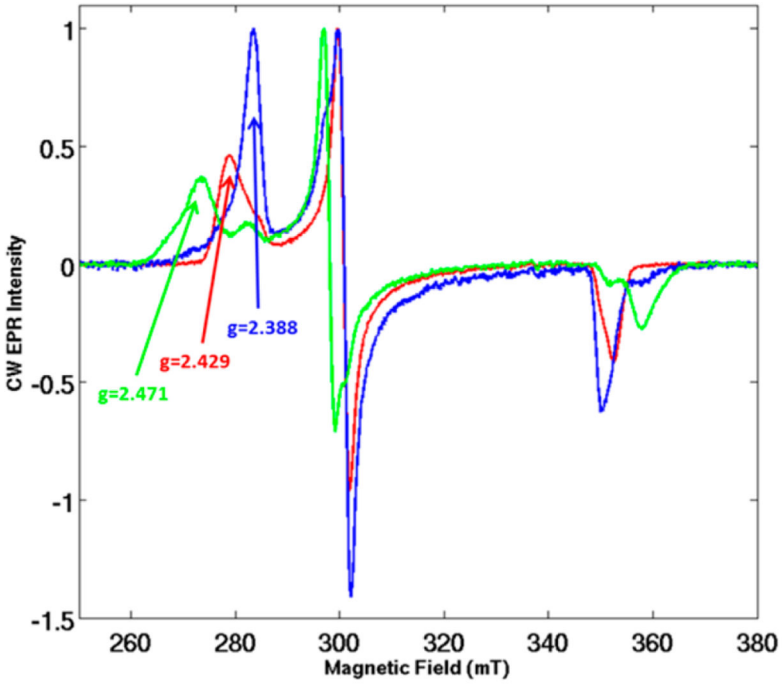

Figure 2.

EPR spectral shifts for CYP2C9d with addition of inhibitor: red, CYP2C9d spectrum with no added drug; green, addition of 1,2,3-TRZ shifts the g_z peak to higher g values (lower field), indicative of water displacement and type II binding; blue, addition of PPT shifts the g_z peak to a lower g value (higher field).

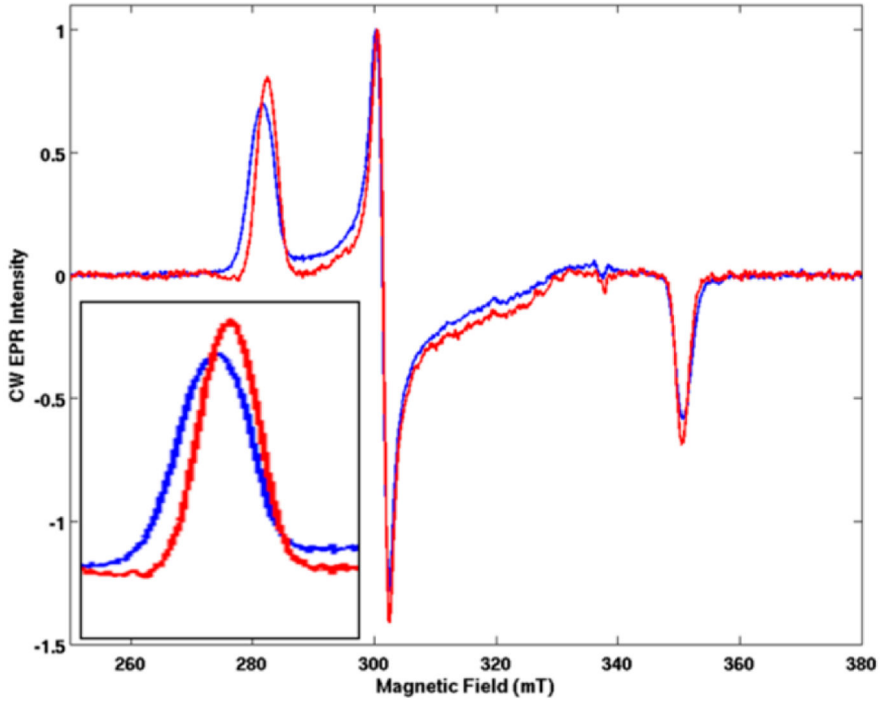

Figure 3.

CW EPR spectrum of CYP125A1 (blue) and in complex with pyridine inhibitor LP10 (red). The inset shows a noticeable sharpening and a shift of the g_z feature.

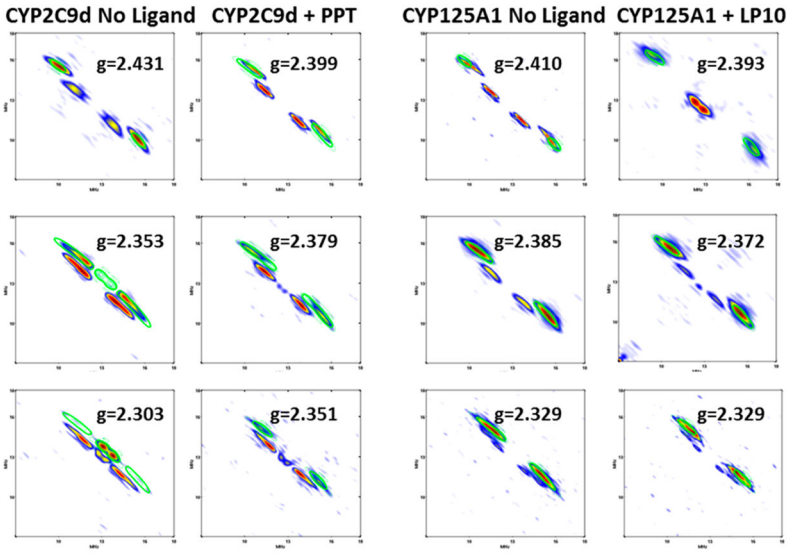

Figure 4.

HYSCORE spectra (multicolor surface) and simulations of the water peaks (green contours) show consistent fits with and without the drug for CYP2C9d and CYP125A1. The parameters used to simulate the HYSCORE spectra are listed in Table 2.

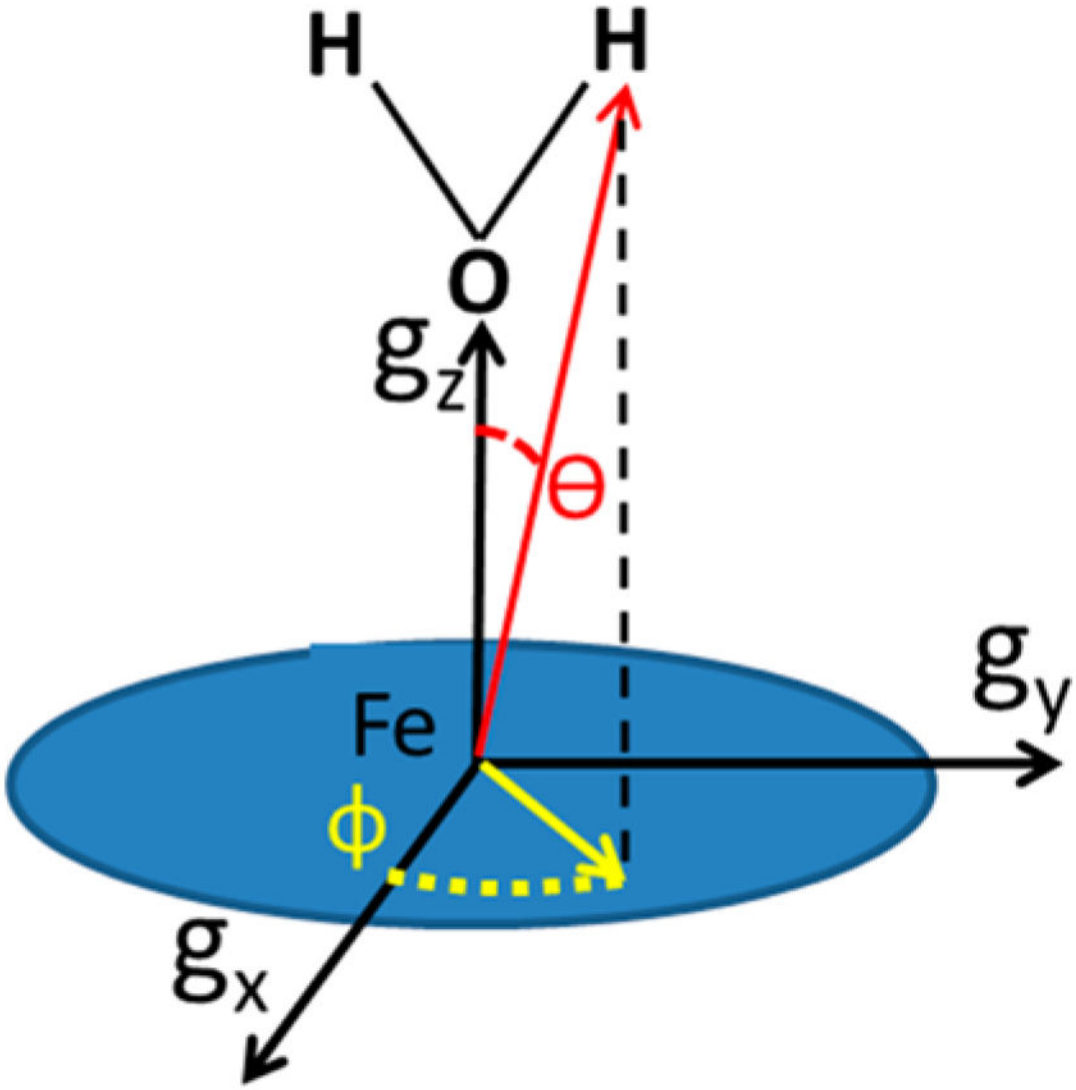

Figure 5.

Definition of the polar angles θ and φ for the hydrogens of the water relative to the g axis system of the heme. The length of the red vector connecting the heme iron and water hydrogen is R.

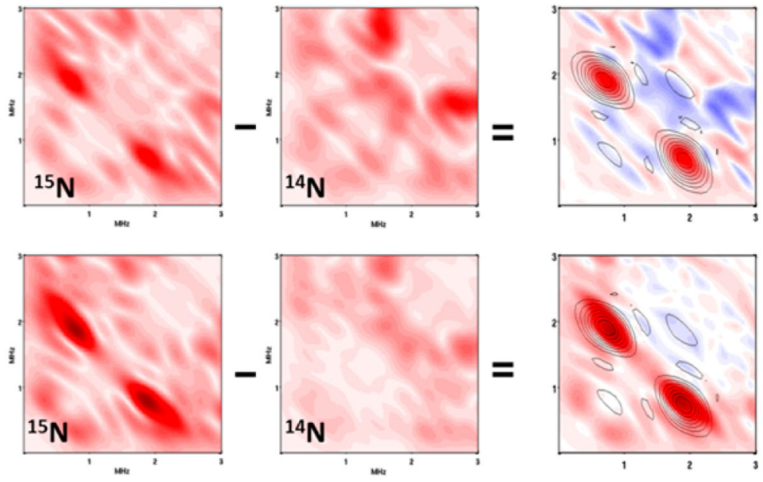

Figure 6.

HYSCORE (left and center) and difference HYSCORE (right) spectra of the CYP2C9–(PPT) complex with [^{15}N]PPT or [^{14}N]PPT at g = 2.396 (top row) and g = 2.376 (bottom row). The black contour lines are simulations using parameters listed in Table 2. In the difference spectra (right), blue indicates negative intensity (decrease of some ^{14}N peaks) and red indicates positive (appearance of ^{15}N peaks).

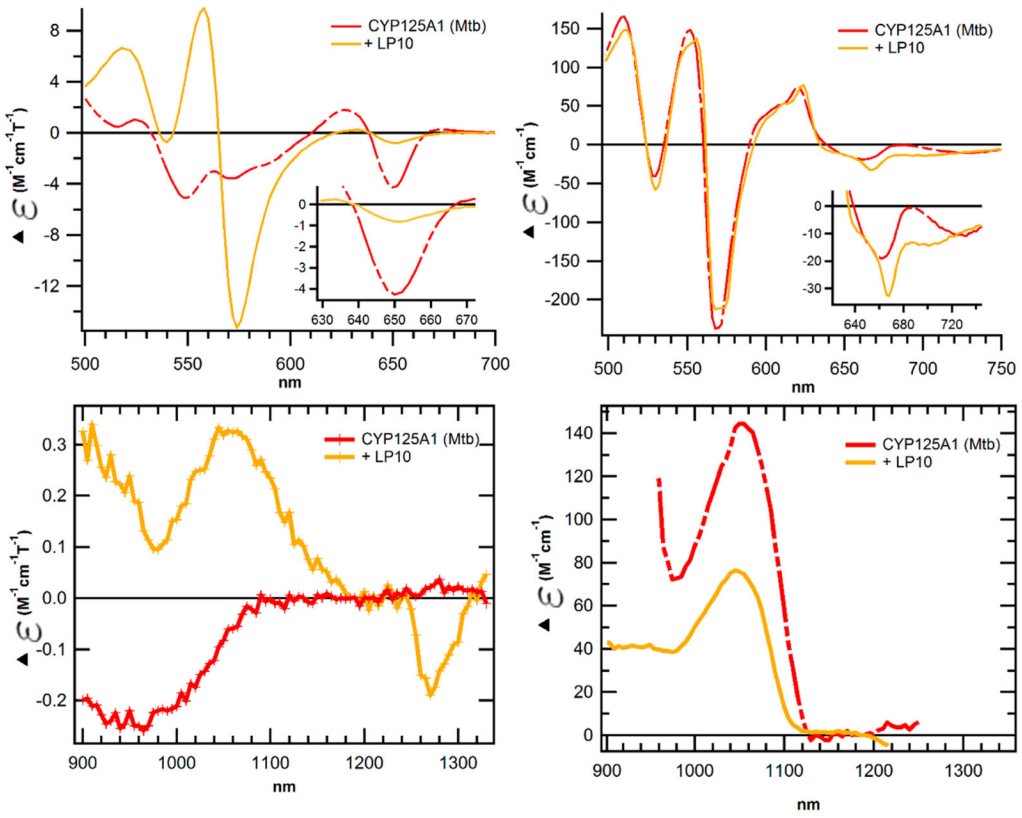

Figure 7.

MCD spectra (6 T) of CYP125A1 (red) and CYP125A1-(LP10) (yellow). The visible MCD spectra are shown at 298 K (top left) and 4.2 K (top right). The corresponding near-infrared spectra at the same temperature are shown in the bottom panels.

Table 1

g Values and Relative Amounts of Species from Fits of the CW EPR Spectra of CYP2C9d

	species	g_z	g_y	g_x	weight (%)
CYP2C9d no drug	**1a**	2.429	2.248	1.917	73
	1b	2.396	2.252	1.929	27
CYP2C9d with PPT	**1a**	2.429	2.248	1.917	20
	1b	2.396	2.252	1.929	14
	2	2.388	2.248	1.930	51
	3a	2.473	2.268	1.895	15
CYP2C9d with 1,2,3-TRZ	**1b**	2.399	2.252	1.923	12
	3a	2.474	2.269	1.899	66
	3b	2.525	2.272	1.881	22

Table 2

Hyperfine Coupling Parameters Obtained from HYSCORE Simulations

	A_{iso} (MHz)	A_{perp} (MHz)	A_{par} (MHz)	θ (±5°)	φ (±5°)	R (nm)
CYP2C9d without drug						
H_2O	−0.67	−4.90	7.80	29°	0°	0.265
CYP2C9d-(PPT)						
H_2O	−0.67	−4.62	7.25	21°	29°	0.271
[^{15}N]PPT	0.80	−0.47	−0.98	–	–	0.444
CYP125A1 without drug						
H_2O	−0.33	−4.35	7.70	26°	23°	0.270
CYP125A1–(LP10)						
H_2O	−0.33	−4.35	7.70	18°	23°	0.270

Table 3

MCD Spectral Parameters of CYP125A1 Complexes at 6 T

no drug, 298 K			LP10, 298 K			no drug, 4.2 K			LP10, 4.2 K		
λ (nm)	$\Delta\varepsilon^a$	type[b]	λ (nm)	$\Delta\varepsilon^a$	type[b]	λ (nm)	$\Delta\varepsilon^a$	type[b]	λ (nm)	$\Delta\varepsilon^a$	type[b]
514	0.53	T	518	6.63	P	510	165.70	P	510	148.20	P
524	1.05	P	558	9.76	P	524		C	524		C
532		C	565		C	528	−40.10	T	530	−58.36	T
548	−5.07	T	574	−15.20	T	535		C	537		C
562	−3.05	P	650	−0.80	M	551	148.44	P	556	137.52	P
610		C	1060	0.32	L	560		C	561		C
626	1.80	P				568	−273.20	T	570	−211.55	T
650	−4.27	M				589		C	592		C
						620	75.16	P	624	76.84	P
						638		C	634		C
						662	−19.13	M	666	−32.16	M
						1050	144.46	L	1045	76.44	L

[a] In units of $(\mathrm{M\ cm\ T})^{-1}$.

[b] Abbreviations: T, trough; P, peak; C, crossover; M, minimum; L, near-IR ligand metal charge transfer.